NANOSYSTEMS:
PHYSICS, CHEMISTRY, MATHEMATICS

Bulyarsky S.V., et al. *Nanosystems: Phys. Chem. Math.*, 2024, **15** (2), 204–214.
http://nanojournal.ifmo.ru
DOI 10.17586/2220-8054-2024-15-2-204-214

Original article

Tunneling recombination in GaN/InGaN LEDs with a single quantum well

Sergey V. Bulyarsky[1], Liubov N. Vostretsova[2], Valeriya A. Ribenek[2]

[1]Institute of Nanotechnology of Microelectronics of the Russian Academy of Sciences (INME RAS), Moscow, Russia

[2]Ulyanovsk State University, Ulyanovsk, Russia

Corresponding author: Liubov N. Vostretsova, kapiton04@yandex.ru

ABSTRACT The paper proposes an analytical model of tunneling-recombination processes with forward and reverse displacements in InGaN/GaN-based structures containing a quantum well, assuming that the processes of generation and recombination are complex, while one of the stages of the transition of the charge carrier to the center is tunneling. Comparing the model with the experiment allowed us to determine the energies of the recombination centers of 0.22 and 0.45 eV. These energies may correspond to centers formed by defect complexes along filamentous dislocations, such as divacansions (V_{Ga} V_N), and a point isolated defect observed in n-type GaN layers grown by various methods, respectively.

KEYWORDS quantum well, nanoscale heterostructures, tunneling recombination, current transfer, nonradiative recombination levels

FOR CITATION Bulyarsky S.V., Vostretsova L.N., Ribenek V.A. Tunneling recombination in GaN/InGaN LEDs with a single quantum well. *Nanosystems: Phys. Chem. Math.*, 2024, **15** (2), 204–214.

1. Introduction

Structures based on InGaN/GaN currently occupy an important place in modern optoelectronics. Light-emitting devices are created based on such structures, operating in the spectral range from green light to near ultraviolet [1]. We can mention displays based on blue and green microLEDs [2–4], as well as communication systems for organizing optical data transmission at a rate of more than 1 Gbit/s [5,6]. LEDs based on III-nitride have many advantages, including high brightness, low power consumption, and long service life [7]. A wide spectral range of radiation has driven the development of microLEDs for displays of mobile devices, such as smart watches, virtual reality devices, and mobile phones [8–10]. The rapid development of the InGaN/GaN technology makes it possible to achieve the required parameters, with high radiation efficiency, reaching up to 90 % [11]. Nevertheless, these LEDs, despite their high efficiency, have high concentrations of defects, both extended and point, and the achieved high material quality enables a more reliable determination of current transfer mechanisms, including those involving defects.

Despite active research on InGaN-based LED structures, the question of the nature of the mechanisms that cause a drop in radiation efficiency during long-term operation remains unsolved. It is believed that the primary cause of the gradual decrease in the emission efficiency of LEDs based on nanoheterostructures is the formation of additional non-radiative recombination centers in the active region [12]. The degradation of SD was explained by the action of macroscopic defects [13], which could lead to the formation of tunneling channels [14] or an increase in contact resistance [15]. In other studies, changes in the characteristics of LED structures during aging are associated with the formation of non-radiative recombination centers in the active region during prolonged current flow. The influence of defects on the degradation characteristics of InGaN/GaN photodetectors with several quantum wells subjected to direct current was investigated [16]. The degradation of electrical and optical characteristics is largely explained by the activation of initially inactive defects, primarily defects associated with Mg–H, C-, and V_{Ga}, in the studied devices, followed by deterioration of their characteristics. These defects stimulate tunnel-recombination transfer of charge carriers with the participation of defects in quantum wells [17, 18], although analytical characteristics describing these processes are currently lacking. Analytical dependences of the current-voltage characteristics of diodes are essential for a deeper understanding of the processes occurring during the transfer of charge carriers and, in some cases, make it possible to determine the parameters of traps in the space charge region of the device [19–21] by using the current-voltage characteristics of the devices for diagnostic purposes. This is facilitated by the models developed [19, 20], which allow one to obtain the parameters of defects involved in tunneling-recombination processes using the analysis of current-voltage characteristics,.

Volt-ampere characteristics are suitable for express diagnostics of recombination centers as they contain complete and important information about defects [20–22], however, it is essential to correctly extract this information from the experiments. The theory of generation and recombination in semiconductor diodes [23, 24] is often underutilized, lacking a thorough understanding of their depth. Several studiesanalyze generation-recombination processes in p-n junctions [25–28] and develop important methods for analyzing these processes. However, a simplified Shockley model is often used,

© Bulyarsky S.V., Vostretsova L.N., Ribenek V.A., 2024

when the cross sections for the capture of electrons and holes to the recombination center are assumed to be the same. This approach is not correct. The injection of electrons and holes changes the occupation of recombination centers with deep levels in the band gap of the semiconductor. Features of the behavior of current-voltage characteristics reflect these processes, revealing the features of the parameters of defects. The influence of the defect parameters enables the discovery of new algorithms for processing current–voltage characteristics (CVCs) [19–23].

The analysis of p-n junction currents under reverse bias is also not well-established and not all available information is extracted from these studies. The diffusion theory of reverse current in p-n junction predicts an absence of dependence on the applied voltage and the activation energy of temperature dependence of diffusion current equal to the band gap of the semiconductor [24]. However, experimental studies show that this is not the case and the energy is less than the band width [21,29]. This indicates the leading role of current generation involving defects [20,21]. To determine the processes governing reverse current, one can examine temperature dependencies. If the experimental value of the activation energy of the current is lower than the energy of the band gap, but greater than half of it, then reverse current is determined by the process of generating electrons and holes through the levels of deep centers. This current is independent of voltage. If voltage dependence occurs, but the activation energy is greater than half of the band, then this is due to the Poole-Frenkel effect [30, 31]. The Poole-Frenkel coefficient has a numerical theoretical value. If the experimental value of this coefficient is greater than the theoretical one, then there is an electron-phonon interaction [21,32]. If the activation energy of the reverse current is less than half the band gap, then tunneling takes part in the formation of the current.

Tunnel processes and generation-recombination processes can occur simultaneously. Therefore, it is necessary to develop diagnostic methods for determining the parameters of the deep centers involved in both processes. The aim of this study is to obtain analytical expressions for the current-voltage characteristics in the case when tunneling and generation-recombination processes simultaneously exist and to use these methods to determine defect parameters in the quantum well of InGaN/GaN LEDs.

2. Samples for research and measurement methods

Commercial shell-less blue-glow LEDs (Taiwan Oasis Technology Co., Ltd) ($\hbar\omega_{\max} = 2.66$ eV, $\lambda_{\max} = 468$ nm at room temperature) with a quantum well (QW) based on InGaN/GaN solid solution were studied.

To achieve this goal, direct volt-ampere (VAC) and volt-capacitive Faraday (VAC) characteristics were measured by an automated measuring system. The measurement of the forward and reverse branches of the HF was carried out in one measuring cycle using a generator-type capacitance meter. The LED under study is switched on in parallel to the LC circuit, the parameters of which are such that in the absence of a sample, the generated frequency is 1 MHz. This measurement scheme makes it possible to achieve an accuracy of measuring the capacitance of ± 0.5 pF.

The measurement of forward and reverse VAC was carried out on an automated measuring complex, which provides for the measurement of low currents using the Picoammeter Keithley 6485. The test sample was fixed to a heating element next to a thermocouple-based temperature sensor. The temperature was maintained with an accuracy of ± 0.5 K.

3. Experimental results

The concentration profile of the dopant (Fig. 1) was determined from the capacitive-voltage characteristic measured at room temperature. The impurity concentration in the space charge region (SCR) was determined as [30]:

$$N = \frac{2}{qS^2\varepsilon\varepsilon_0}\left[-\frac{1}{\frac{d(1/C^2)}{dU}}\right], \tag{1}$$

where e is the electron charge, S is the area of the structure (cm^2), ε is the dielectric permittivity of GaN, ε_0 is the dielectric constant (V/cm), q is the electron charge, C is the capacitance of the structure, and U is the voltage across the sample.

Current-voltage characteristics at forward bias, measured under various temperatures, are presented in Fig. 2.

To determine the mechanism of current transfer in the studied structures, the dependence at $I = f\left(\frac{1}{T}\right)$ a fixed forward voltage on the sample was used [19,21] (Fig. 3).

Figure 4 shows the dependence of the activation energy on the forward bias voltage. As seen from Fig. 4, the activation energy E_a at a forward bias voltage below the forward bias $(E_g - qU)/2$ over the entire range of forward bias voltages is less than 2 V, therefore, tunneling current predominates in this voltage range [19, 21]. The activation energy determined from the slope of the curves in Fig. 2, ranges from 0.2 to 0.4 eV depending on the bias voltage, which is significantly lower than half the potential barrier, which is determined by $(E_g - qU)/2$ (Fig. 4). This value is much less than $0.5A_g$, but greater than zero. Such a change in energy is typical for tunnel-recombination processes.

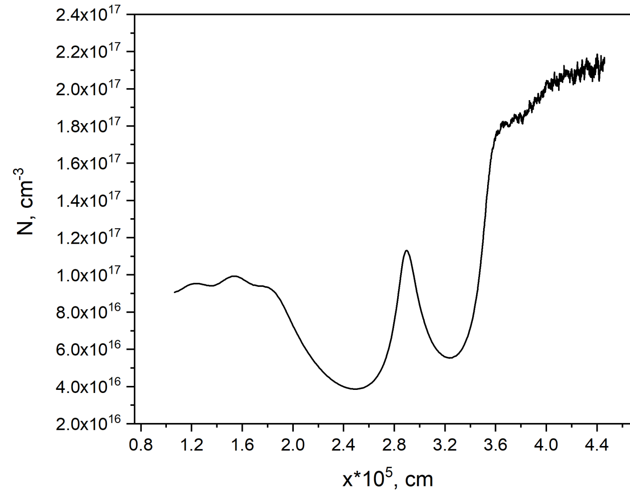

FIG. 1. Dopant distribution profile in the studied structure (1). Calculation of the concentration profile based on the results of capacitance-voltage measurements indicates the presence of a single quantum well with a width of approximately 40 nm.

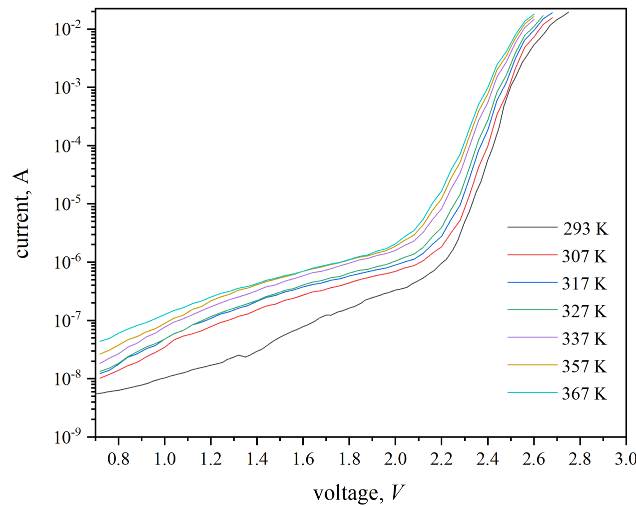

FIG. 2. Forward-biased current-voltage characteristics of InGaN/GaN LEDs, measured in the temperature range of 293 – 367 K. The change in the current value with temperature occurs quite weakly, indicating the influence of tunneling processes on charge transport.

4. Analysis of tunnel-recombination processes

Tunnel-recombination processes have been analyzed in [19, 20], where expressions for the recombination rate and various approximations of current-voltage characteristics were obtained. In this study, we propose a simpler and more convenient approach for analysis. We will adhere to the model that electrons from the conduction band tunnel into the well, and holes are injected from the p-region and are captured within it. Recombination occurs in the quantum well (QW). The transition model is shown in Fig. 5. It is important to note that this model is only valid in the initial part of the current-voltage characteristic, as long as the number of electrons injected from the conduction band is less than the number of electrons tunneling from it into the QW. In our case, this is the CVC region (Fig. 1) at voltages less than 2 V.

Taking into account that the level is closer to the conduction band and there is no emission from the center in the well to the valence band, we conclude that the hole recombination rate is equal to:

$$\frac{dp}{dt} = -c_p p n_t, \tag{2}$$

where c_p is the coefficient of hole capture by recombination centers in the QW; n_t is the electron concentration at the recombination centers in the QW.

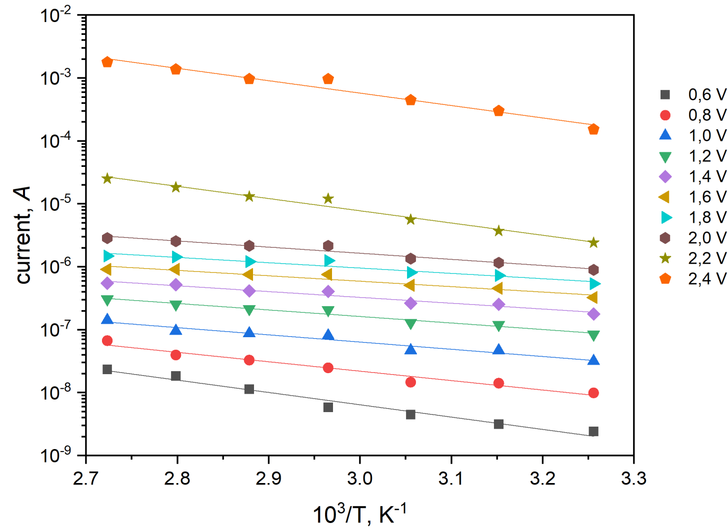

FIG. 3. Temperature dependences of the direct current at a voltage across the sample in the range of 0.6 – 2.4 V (with a step of 0.2 V). By dependence $I = f(1/T)$ the activation energy of current transfer was determined as $E_a = k \cdot \tan\alpha$, where k is the Boltzmann constant.

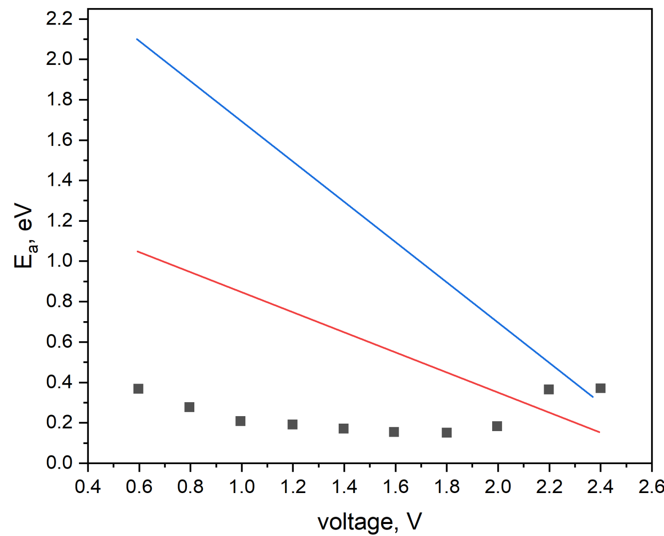

FIG. 4. Dependence of current activation energy on forward bias voltage: 1 – experimental value $E_a = f(U)$; 2 – $\frac{E_g - qU}{2}$; 3 – $E_g - qU$ (E_g – band gap, q – electron charge). The activation energy varies in the range from 0.2 to 0.4 eV, depending on the bias voltage. This value is much less than half the width of the InGaN band gap, but greater than zero, which is typical for tunnel recombination processes.

Electron tunneling rate:

$$\frac{dn}{dt} = -w_t n \left(N_t - n_t\right), \tag{3}$$

where w_t is the probability of electron tunneling from the conduction band to recombination centers in the QW; N_t is the concentration of recombination centers in the QW.

We equate these rates and obtain the probability of filling the traps and the rate of recombination with their participation:

$$\frac{dn_t}{N_t} = \frac{w_t n}{c_p p + w_t n}, \qquad R = \frac{dp}{dt} = -\frac{c_p p w_t n}{c_p p + w_t n} N_t. \tag{4}$$

The recombination current density is found as

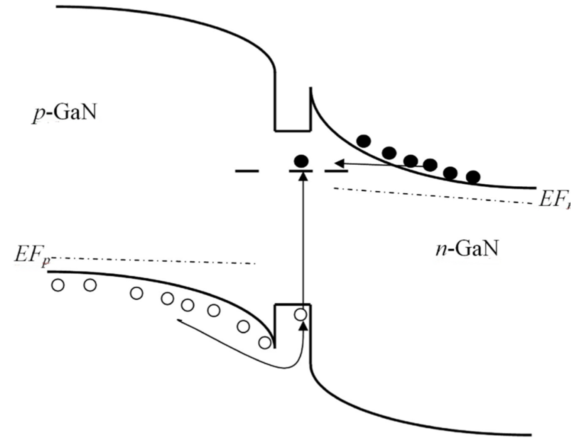

FIG. 5. Tunneling recombination model InGaN/GaN at forward bias. Electrons from the conduction band tunnel into the quantum well, and holes are injected from the p-region and trapped in the quantum well region.

$$j = e\int\limits_{x_p}^{x_n} R\left(x\right)dx, \tag{5}$$

where x_n, x_p are the boundaries of the space charge region (SCR).

The coordinate dependence of the recombination rate is a bell-shaped function with almost exponential wings [19]. The current value is determined by the maximum recombination rate. Integral (4) is calculated assuming that the recombination rate is the same at all points of the SCR and is equal to the maximum, then

$$j = q\int\limits_{x_p}^{x_n} R\left(x\right)dx = q\int\limits_{x_p}^{x_n} R_{\max}dx = qR_{\max}\int\limits_{x_p}^{x_n} dx = eR_{\max}\left(x_n - x_p\right) = qR_{\max}d, \tag{6}$$

where d is the SCR width, which can be calculated from the capacitance-voltage characteristics.

The value of the tunnel-recombination current can be obtained taking into account (6), (4). It is equal to

$$j = qdR_{\max} = qd\frac{c_p p w_t n}{c_p p + w_t n}N_t. \tag{7}$$

The probability of tunneling through a triangular barrier is given by the Fowler–Norheim formulas

$$w_t = \frac{I}{qdnS} = \frac{KF^2}{qdnS}\exp\left(-\frac{b\left(E_t - E_f - qU\right)^{3/2}}{F}\right), \tag{8}$$

where S is the area of p-n junction; F is the electric field strength; E_t is the activation energy of the level of recombination centers, measured from the conduction band; E_f is the Fermi energy,

$$a = \frac{q^3}{8\pi h} = 1.541\cdot 10^{-6}S\ \left[\text{eV/V}^2\right],$$

$$b = \frac{8\pi}{3(2m^*)^{0.5}/qh} = 6.831\cdot 10^9\ \left[\text{eV}^{-3/2}\text{V/m}\right].$$

The probability of tunneling for one electron is determined from formula (8):

$$w_t n = \frac{I}{qdS} = \frac{KF^2}{qdS}\exp\left(-\frac{b\left(E_t - E_f - qU\right)^{3/2}}{F}\right). \tag{9}$$

Then the current is as follows

$$j = qdR_{\max} = qd\frac{c_p p w_t n}{c_p p + w_t n}N_t = \frac{c_p p\frac{KF^2}{S}\exp\left(-\frac{b(E_t - E_f - qU)^{3/2}}{F}\right)}{c_p p + \frac{KF^2}{qdS}\exp\left(-\frac{b(E_t - E_f - qU)^{3/2}}{F}\right)}N_t. \tag{10}$$

Holes overcome the potential barrier $E_p = \dfrac{(V_d - qU)}{2}$, where V_d is the diffusion potential, in our case 2.7 eV.

Then,

$$j = qdR_{\max} = qd\frac{c_p p w_t n}{c_p p + w_t n} N_t = \frac{c_p p_p \exp\left(-\frac{V_d - qU}{2kT}\right) \frac{KF^2}{S} \exp\left(-\frac{b(E_t - E_f - qU)^{3/2}}{F}\right)}{c_p p_p \exp\left(-\frac{V_d - qU}{2kT}\right) + \frac{KF^2}{qdS} \exp\left(-\frac{b(E_t - E_f - qU)^{3/2}}{F}\right)} N_t. \quad (11)$$

When modeling using expression (11), the fitting parameters are the constant K, the hole capture coefficient c_p and $E_t - F_f$. The magnitude of the electric field F and the width of the SPV d were determined from capacitance-voltage characteristics. The concentration of holes in the p-region, p_p , assumed equal to the concentration of a fine impurity determined from the impurity distribution profile (Fig. 1). The energies in (11) are measured from the bottom of the conduction band in n-GaN. The position of the Fermi level in n-GaN was taken 0.7 ± 0.1 eV [33].

The simulation results are shown in Fig. 6. Comparison of calculations with the experiment made it possible to determine the activation energies of the recombination centers 0.22 ± 0.05 eV and 0.45 ± 0.05 eV.

The level with the energy of 0.22 eV in the conduction band was interpreted as defect complexes along filamentary dislocations, such as divacancies (V_{Ga} V_N) [34]. The level with the energy of 0.45 eV is treated as a point isolated defect, which is observed in GaN layers n-type grown by different methods [35].

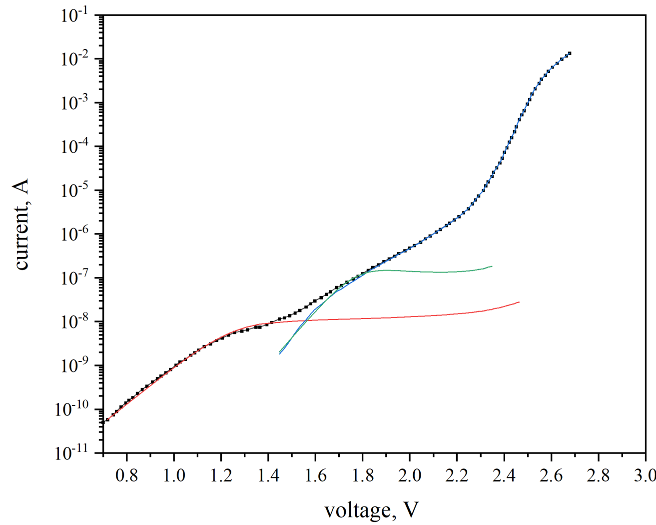

FIG. 6. Simulation of tunnel-recombination currents of InGaN/GaN LEDs under forward bias. The simulation of (11) made it possible to determine the activation energies of the recombination centers of 0.22 ± 0.05 eV (purple line) and 0.45 ± 0.05 eV (green line).

It is believed that the mechanism of the flow of direct current can be estimated by the differential indicator of the slope of the CVC (ideality factor)

$$\beta = \frac{qI}{kT}\left(\frac{dI}{dU}\right)^{-1} = \frac{q}{kT}\left(\frac{d\ln I}{dU}\right)^{-1}. \quad (12)$$

Figure 7 shows the results of calculating this parameter from equation (10) and the same parameter calculated from the experimental I–V characteristics. These values reach their maximum at the same voltage. The value of this exponent significantly exceeds the value of 2, which follows from the theory of Shockley, Noyce, and Saa [24]. This result shows that the theoretical CVC (11), obtained on the basis of the model in Fig. 6 describes the experimental results quite well, and the value of $\beta > 2$ indicates the participation of tunneling mechanism in the formation of the forward current of the LEDs.

5. Current-voltage characteristics with reverse bias

The activation energies of the reverse current were calculated for various electric field strengths. These results are shown in Fig. 8 ($E = f(F^{1/2})$):

The straight line in Fig. 8 is an approximation of the experimental data by the expression:

$$E = E_t - \beta_{\exp}\sqrt{F} = 0.47 - 3.6 \cdot 10^{-4}\sqrt{F}. \quad (13)$$

Thus, the energy of the energy level of defects through which generation occurs is 0.47 eV, and the experimental value of the Poole-Frenkel coefficient $\beta_{\exp} = 3.6 \cdot 10^{-4}$ eV/(B/cm). The activation energy is less than half the band gap. This fact allows us to assume the following reverse current flow model, namely: holes tunnel from a trap that forms an energy level from which electrons are generated into the conduction band (Fig. 9). In this case, the generation energy is less than half of the band gap.

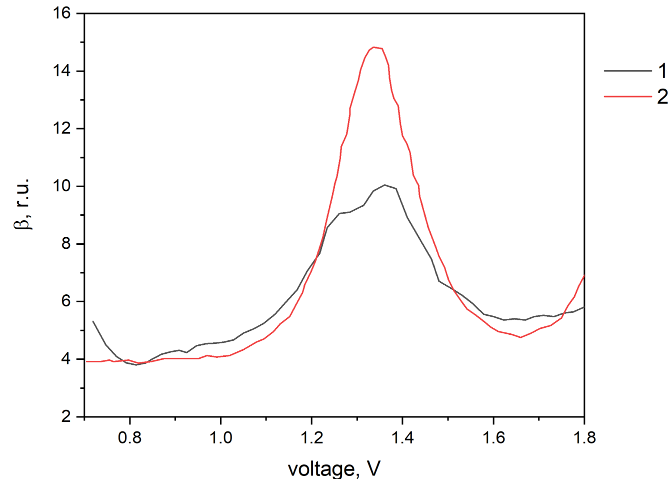

FIG. 7. Addiction $\beta = f(U)$ for the structure under study at room temperature: 1 – experimental dependence (12); 2 – calculation taking into account (11). The value $\beta > 2$ indicates the involvement of the tunneling mechanism in the formation of direct current of LEDs.

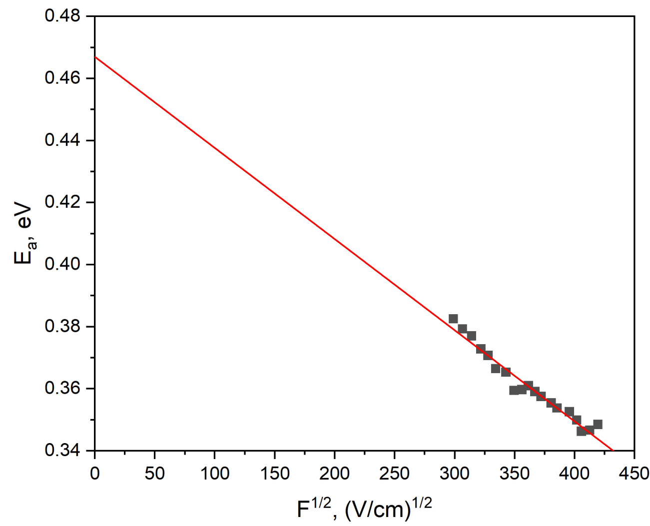

FIG. 8. Dependence of the activation energy of the inverse current-voltage characteristics on the electric field strength in the space charge region. Inverse current-voltage characteristics plotted in coordinates $\ln(I) = f\left(F^{1/2}\right)$ are linear. This is the characteristics of the Poole-Frenkel effect, which reduces the generation barrier height proportionally to the root of the electric field strength [21].

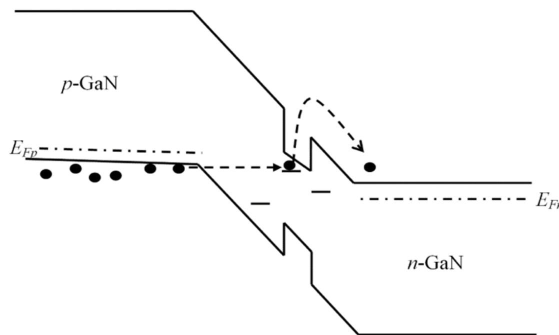

FIG. 9. Tunneling recombination model InGaN/GaN under reverse bias. The holes tunnel out of the trap, forming an energy level from which electrons are generated into the conduction band.

At a reverse voltage, the space-charge region of the p-n junction (SCR) is depleted of free charge carriers, and the equilibrium between recombination and generation is shifted towards generation. The reverse current, as well as the direct current, is determined by expression (5).

Let's consider the recombination rate in the case when one transition is the tunneling of a hole from the valence band to a level, and the second transition is the generation of electrons in the conduction band. Let the processes occur under reverse bias. In this case, the space-charge region is depleted of electrons and holes, and there are no captures of charge carriers at recombination centers. Under this condition, this velocity can be found from the system of kinetic equations:

$$\begin{aligned} R_n &= \frac{dn}{dt} = -c_n n\left(N_t - n_t\right) + e_n^t n_t, \\ R_p &= \frac{dp}{dt} = -c_p p n_t + w_p(N_t - n_t), \end{aligned} \tag{14}$$

where N_t is the concentration of deep centers, n_t is the concentration of electrons at them; e_n^t is the speed of electron emission from a deep level; w_p is the probability of hole tunneling from the valence band to a deep level.

The equilibrium condition takes place $R = R_n = R_p$ for stationary current. The recombination rate is found from (13) under the condition $n = 0$ and $p = 0$ fair with a reverse bias, we obtain:

$$I_{rev} = qA\int_0^w \frac{e_n^t(x)w_p(x)N_t(x)}{e_n^t(x) + w_p(x)}dx, \tag{15}$$

where $e_n^t = \gamma_n c_n N_c \exp\left(-\frac{(E_c - E_t)}{kT}\right)$, γ_n is the degeneracy factor of the level of the deep center for electrons and holes. These factors vary from 0.5 to 2.

In our case, the following facts take place: firstly, there is a significant temperature dependence of the current, and secondly, the activation energy is less than half of the band gap. Taking these experimental facts into account, we can assume that the tunneling probability $w_p \gg e_n^t$ is much higher than the recombination rate, and the level of the deep center is located closer to the conduction band

$$I_{rev} = qAw(U)N_t e_n^t. \tag{16}$$

From the conclusions made above and from formula (15), the expression for the current-voltage characteristics of the p-n junction with reverse bias is calculated:

$$I_{rev} = qAe_{n0}^t\int_0^w N_t(x)\exp\left(\frac{\Delta E_t(x)}{kT}\right)dx = qAe_{n0}^t\int_0^w N_t(x)\exp\left(\frac{\beta_F\sqrt{F(x)}}{kT}\right)dx, \tag{17}$$

where e_{n0}^t is the speed of electron emission without taking into account the influence of the electric field. Fig. 10 shows the inverse volt-ampere characteristic in coordinates $I = f(F^{1/2})$.

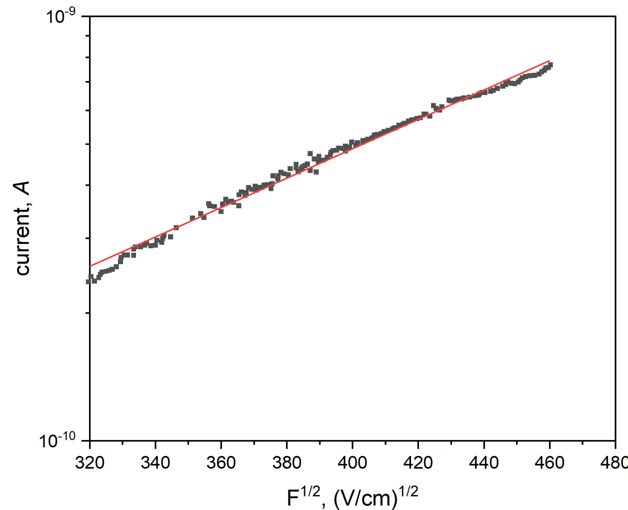

FIG. 10. Dependence of the reverse current on $F^{1/2}$ for the structure under study at room temperature. The dependence of the reverse current on $F^{1/2}$ on a logarithmic scale is close to linear, which confirms the validity of the expression used in the work [16].

The theoretical value of the Frenkel-Pool constant ($\beta_F = q^{3/2}/\sqrt{\pi\varepsilon\varepsilon_0}$) is equal to 2.3 eV·$10^{-4}$ cm$^{1/2}$/V$^{1/2}$. The reason for the discrepancy between this value and the value determined experimentally is the electron-phonon interaction. In the work of S. F. Timashev showed that [32]:

$$\beta_{Fex} = \beta_F\left(1 + \frac{E_0 - S\hbar\omega}{2S\hbar\omega}\right), \tag{18}$$

where $S\hbar\omega$ is a value equal to half of the heat release that accompanies the electron-phonon interaction; E_0 is the energy of a purely electronic transition, S is the Huang and Ries factor, $h\omega$ is the energy of the characteristic phonon in the one-coordinate model.

The model of electron-phonon interaction, which takes into account interactions with a single phonon, gives the value for the thermal transition energy of charge carrier generation [20, 21]:

$$E_t = \frac{(E_0 + S\hbar\omega)^2}{4S\hbar\omega}. \tag{19}$$

The numerical values of the activation energy and the experimental Poole-Frenkel constant are known. Parameters of the electron-phonon interaction $S\hbar\omega$ and E_0 are determined by jointly solving equations (17) and (18). They are equal to $E_0 = 0.40$ eV, and $S\hbar\omega = 0.19$ eV. These parameters determine the potentials of the configuration-coordinate diagram:

$$U_g = \frac{\hbar\omega Q^2}{2}; \quad U_u = \frac{\hbar\omega\left(Q - Q_0\right)^2}{2} + E_0, \tag{20}$$

where $Q_0 = \sqrt{2S}$, and Q is the current coordinate of the x-axis. Using the obtained parameters, we build a configuration-coordinate diagram of the generation center (Fig. 11).

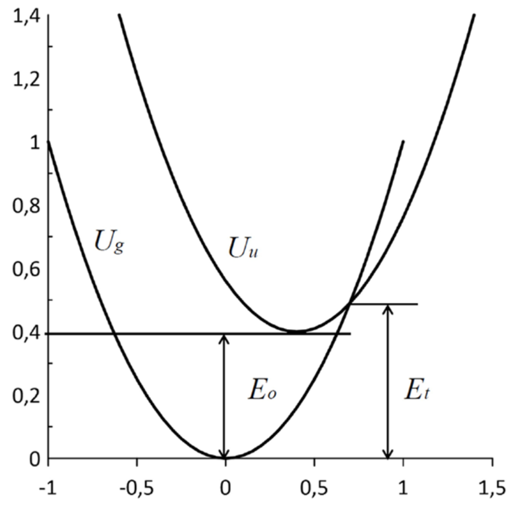

FIG. 11. Configuration-coordinate diagram of the center from which electrons are generated into the conduction band

6. Conclusion

This work proposes an analytical model of tunneling-recombination processes under forward and reverse biases, assuming that the processes of generation and recombination have a complex nature, with one of the stages of transition of the charge carrier to the center being tunneling. Under forward bias, an electron from the conduction band tunnels to the recombination center in the QW through a triangular barrier, and holes are injected from the p-region and are captured by the recombination center in the QW. This model is valid when the flux of tunneling electrons exceeds the flux of injected electrons from the conduction band. Comparison of the model with experiment made it possible to determine the energies of recombination centers in QWs, 0.22 and 0.45 eV. These energies can correspond to the centers formed by defect complexes along filamentary dislocations, such as divacancies ((VGa VN), and a point isolated defect, which is observed in n-type GaN layers grown by various methods, respectively.

In case of reverse displacement, the following current transfer model is proposed: a hole tunnels from a trap forming an energy level in the band gap into the valence band, while an electron is generated into the conduction band. By solving kinetic equations (13) corresponding to the proposed model, an expression for the inverse characteristics of the studied structures (16) is obtained. According to (16), the reverse current exponentially depends on F (F is the electric field strength), which is confirmed experimentally (Fig. 10).

References

[1] DenBaars S.P. Development of gallium-nitride-based light-emitting diodes (LEDs) and laser diodes for energy-efficient lighting and displays. *Acta Materialia*, 2013, **61**, P. 945–951.

[2] Huang Y., Hsiang E.-L., Deng M.-Y., Wu S.-T. Mini-LED, Micro-LED and OLED displays: present status and future perspectives. *Light: Science & Applications*, 2020, **9**, 105.

[3] Parbrook P.J., Corbett B., Han J., Seong T.-Y., Amano H. Micro-Light Emitting Diode: From Chips to Applications. *Laser & Photonics Reviews*, 2021, **15**, 2000133

[4] Lee S.-L., Cheng C.-C., Liu C.-J., Yeh C.-N., Lin Y.-C. 9.4-inch 228-ppi flexible micro-LED display. *J. of Society for Information Display*, 2021, **29**, P. 360–369.

[5] Shi J.W., Chi K.L., Wun J.M., Bowers J.E., Sheu J.K. GaN based Cyan light-emitting diodes with GHz bandwidth. *IEEE Photonics Conf. IPC, IEEE*, Piscataway, NJ, 2016, P. 623–624.

[6] Pepe A., Chen C.-J., Fu H.Y., Chen K.-C., Wang L., Wang L., Zhang L., Wu M.-C., Liu X., Luo Y., Dong Y., Wei Z., Wang L., Luo Y., Fu H.Y. 2 Gbps/3 m air–underwater optical wireless communication based on a single-layer quantum dot blue micro-LED. *Optics Letters*, 2020, **45**, P. 2616–2619.

[7] Kou J., Shen Ch.-Ch., Shao H. Impact of the surface recombination on InGaN"/ GaN-based blue micro-light emitting diodes. *Optics Express*, 2019, **27** (12), A643–A653 .

[8] Wu T., Sher C.-W., Lin Y., Lee C.-F., Liang S., Lu Y., Huang Chen S.-W., Guo W., Kuo H.-C., Chen Z. Mini-LED and Micro-LED: Promising Candidates for the Next Generation Display Technology. *Applied Sciences*, 2018, **8** (9), 1557.

[9] Zhang K., Peng D., Chong W.C., Lau K.M., Liu Z. Investigation of Photon-Generated Leakage Current for High-Performance Active Matrix Micro-LED Displays. *IEEE Transactions on Electron Devices*, 2016, **63** (12), P. 4832–4838.

[10] Liu Z., Chong W.C., Wong K.M., Lau K.M. GaN-based LED micro-displays for wearable applications. *Microelectronic Engineering*, 2015, **148**, P. 98–103.

[11] David A., Young N.G., Lund C., Craven M.D. Review—The Physics of Recombinations in III-Nitride Emitters. *ECS J. of Solid State Science and Technology*, 2020, **9** (1), 016021.

[12] Seong T.-Y., Han J., Amano H., Morkoç H. *III-Nitride Based Light Emitting Diodes and Applications*. Springer Nature Singapore Pte Ltd XI, 2017, **495**.

[13] Gong Z., Gaevski M., Adivarahan V., Sun W., Shatalov M., Asif Khan M. Optical power degradation mechanisms in AlGaN-based 280 nm deep ultraviolet light-emitting diodes on sapphire. *Applied Physics Letters*, 2006, **88**, 121106

[14] Pinos A., Marcinkevicius S., Shur M.S. High current-induced degradation of AlGaN ultraviolet light emitting diodes. *J. Appl. Phys.*, 2011, **109**, 103108.

[15] Meneghini M., Barbisan D., Bilenko Y., Shatalov M., Yang J., Gaska R., Meneghesso G., Zanoni E. Defect-related degradation of Deep-UV-LEDs. *Microelectronics Reliability*, 2010, **50**, 1538.

[16] Dalapati P., Yamamoto K., Egawa T., Miyoshi M. Impact of current-induced degradation process on the electro-optical characteristics of InGaN/GaN multiple-quantum-well photodetectors fabricated on sapphire substrate. *Applied Physics Letters*, 2021, **118**, 021101.

[17] Bochkareva N.I., Shreter Y.G. Effect of Deep Centers on Charge-Carrier Confinement in InGaN/GaN Quantum Wells and on LED Efficiency. *Semiconductors*, 2018, **52** (7), P. 934–941.

[18] Bochkareva N.I., Rebane Y.T., Shreter Y.G. Efficiency Droop in GaN LEDs at High Current Densities: Tunneling Leakage Currents and Incomplete Lateral Carrier Localization in InGaN/GaN Quantum Wells. *Semiconductors*, 2014, **48** (8), P. 1079–1087.

[19] Bulyarsky S.V., Rud' Yu.V., Vostretsova L.N., Kagarmanov A.S., Trifonov O.Yu. Tunneling recombination in semiconductor structures with nanodisordering. *Semiconductors*, 2009, **43** (4), P. 440–446.

[20] Bulyarskiy S.V. Generation and Recombination Processes in Disordered Semiconductor Structures with Deep Centers. *Global J. of Science Frontier Research: A Physics and Space Science*, 2020, **20** (13).

[21] Bulyarskiy S.V. The effect of electron-phonon interaction on the formation of reverse currents of pn-junctions of silicon-based power semiconductor devices. *Solid State Electronics*, 2019, **160**, 107624

[22] Bulyarskiy S.V., Lakalin A.V., Abanin I.E., Amelichev V.V., Svetuhin V.V. Optimization of the parameters of power sources excited by β-radiation. *Semiconductors*, 2017, **51** (1), P. 66–72.

[23] Shockley W. The theory of pn-Junctions in semiconductors and pn-Junction transistors. *Bell System Technical J.*, 1949, **28** (3), P. 435–489.

[24] Sah C.T., Noyce R.N., Shockley W. Carrier Generation and Recombination in PN Junctions and PN Junction Characteristics. *Proceedings of the IRE*, 1957, **45** (9), P. 1228–1243.

[25] Rein S., Rehrl T., Warta W., Glunz S.W. Lifetime spectroscopy for defect characterization: Systematic analysis of the possibilities and restrictions. *J. of Applied Physics*, 2002, **91**, P. 2059–2070.

[26] Simoen E., Claeys C., Vanhellemont J. Defect Analysis in Semiconductor Materials Based on pn Junction Diode Characteristics. *Defect and Diffusion Forum*, 2007, **261–262**, P. 1–24.

[27] Simoen E., Claeys C. On the impact of the capture rates on the generation/recombination lifetime ratio of a single deep level. *IEEE Transactions on Electron Devices*, 1999, **46**, P. 1487–1488.

[28] Macdonald D., Cuevas A. Validity of simplified Shockley-Read-Hall statistics for modeling carrier lifetimes in crystalline silicon. *Physical Review B*, 2003, **67**, 075203.

[29] Al Abdullah K., Al Alloush F., Jaafar A., Salame C. Study of the effects related to the electric reverse stress currents on the Mono-Si solar cell electrical parameters. *Energy Procedia*, 2013, **36**, P. 104–113.

[30] Shan Q., Meyaard D.S., Dai Q., Cho J., Fred Schubert E., Kon Son J., Sone C. Transport-mechanism analysis of the reverse leakage current in GaInN light-emitting diodes. *Applied Physics Letters*, 2011, **99**, 253506.

[31] Musolino M., van Treeck D., Tahraoui A., Scarparo L., De Santi C., Meneghini M., Zanoni E., Geelhaar L., Riechert H. A physical model for the reverse leakage current in (In,Ga)N/GaN light-emitting diodes based on nanowires. *J. of Applied Physics*, 2016, **119** (4), 044502.

[32] Timashev S.F. On the Frenkel effect during thermofield ionization of deep centers in the space charge layer in semiconductors. *Phys Solid State*, 1974, **16**, P. 804–811.

[33] Rickert K.A., Ellis A.B., Kim J.K., Lee J.-L., Himpsel F.J., Dwikusuma F., Kuech T.F. X-ray photoemission determination of the Schottky barrier height of metal contacts to n-GaN and p-GaN. *J. of Applied Physics*, 2002, **92** (11), 6671.

[34] Narita T., Tokuda Y. Deep levels in GaN. in T. Narita, T. Kachi, (eds.), *Characterization of Defects and Deep Levels for GaN Power Devices*, Melville, New York: AIP Publishing, 2020, P. 3-1–3-36.

[35] Krtschil A., Witte H., Lisker M., Christen J., Krost A., Birkle U., Einfeldt S., Hommel D., Scholz F., Off J., Stutzmann M. Photoelectric properties of the 0.44 eV deep level-to-band transition in gallium nitride investigate by optical admittance spectroscopy. *Applied Physics Letters*, 2000, **77** (4), 546.

Submitted 25 January 2024; revised 10 March 2024; accepted 11 March 2024

Information about the authors:

Sergey V. Bulyarsky – Institute of Nanotechnology of Microelectronics of the Russian Academy of Sciences (INME RAS), Leninskiy prospect, 32A, Moscow 119991, Russia; ORCID 0000-0002-9777-746X; dimka97@mail.ru

Liubov N. Vostretsova – Ulyanovsk State University, Tolstoy street, 42, Ulyanovsk 432097, Russia; ORCID 0000-0001-9602-0812; kapiton04@yandex.ru

Valeriya A. Ribenek – Ulyanovsk State University, Tolstoy street, 42, Ulyanovsk 432097, Russia; ORCID 0000-0002-9233-5339; ribl98@mail.ru

Conflict of interest: the authors declare no conflict of interest.